# Input Voltage Control Scheme for High Efficiency Operation of Multi-axis High-Precision Wireless Powered Stage

Ryunosuke Katada* Student Member,
Takehiro Imura* Member,
Koichi Sakata** Senior Member,
Zhaoxiang Chen** Non-member,
Kazuhiro Suzuki** Non-member
Yuma Yazaki* Student Member
Hiroshi Fujimoto* Senior Member
Atsushi Hara** Non-member
Kazuhiro Yokoyama** Non-member

The most serious problem encountered in the high-precision stages of manufacturing semiconductors and liquid crystal displays is cable disturbance caused by power lines and communication lines connected between the power supply and stages. In our group, a multi-axis high-precision stage without cable disturbance was developed by adopting magnetic resonance coupling wireless power transfer. This study proposes an input voltage control scheme considering the power trajectory for a higher efficiency of the proposed stage stage and evaluates the effectiveness of the proposed method through simulations and experiments.

**Keywords:** wireless power transfer, magnetic resonance coupling, multi-axis high precision stage, power transfer efficiency

## 1. Introduction

Semiconductors and flat panel liquid crystal displays (LCDs) are manufactured through high-precision stages. It is important to improve the tracking performance of these high-precision stages to make them more precise and faster. Fig.1 shows the causes of tracking errors. To reduce tracking errors, various studies were done from many aspects such as control [1] and structure [2]. Among these causes, cable disturbance caused by power lines and communication lines connected between the power supply and stages is the most serious cause of tracking errors in the high-precision stages [3], [4]. It is important to suppress cable disturbance to reduce the magnitude of the tracking error. For this purpose, our group developed a one-axis and two-axis wireless high-precision stages (WHPSs). These stages utilize wireless power transfer. Cable disturbance caused by power lines and communication lines was eliminated through wireless transmission of the required power, as shown in Fig. 2. This study proposes an efficient input voltage control scheme, which, unlike Wireless In-Wheel Motors [5], [6], is based on the power trajectory of the high-precision stage for the two-axis WHPS.

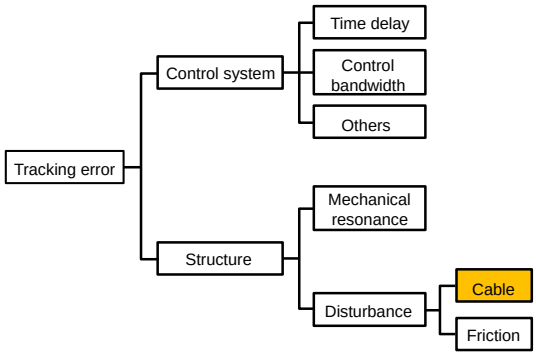


Fig. 1. Causes of tracking error

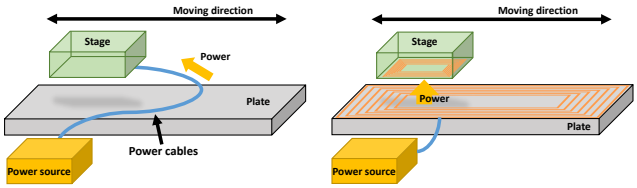


(a)Conventional stage (b)Wireless powered stage

Fig. 2. A conceptual image of the stages

## 2. Multi-axis wireless high precision stage

### 2.1 WPT using magnetic resonance coupling

Wireless power transfer (WPT) technologies have attracted much attention because of their diverse applications such as EV charging, IoT devices, and industrial machinery. Magnetic resonance coupling is the most popular method because of its ability to to transmit power over long distances with high efficiency [7]. For this WPT method, the resonance frequencies should be identical on the primary and secondary side. The resonance frequency can be adjusted using compensation capacitors.

Fig.3 shows a basic equivalent circuit of a series-series (SS) topology WPT system, in which the compensation ca-

* The University of Tokyo, 5-1-5, Kashiwanoha, Kashiwa, Chiba, 227-8561 Japan
** Nikon cooperation, 471, Nagaodaityou, Sakae, Yokohama, Kanagawa, 244-8853, Japan

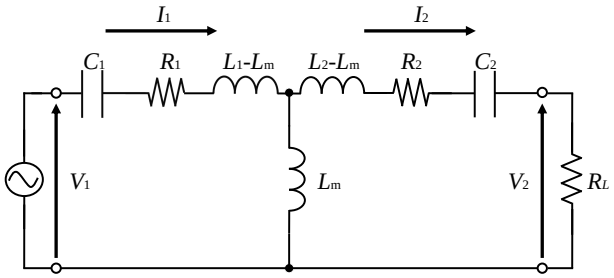


Fig. 3. Basic equivalent circuit of SS topology WPT system

pacitors are connected in series on both the primary and secondary sides. In Fig. 3, $R$, $L$, $C$ denote the resistance, inductance, and capacitance, respectively. $L_m$ is the mutual inductance of the two coils, and $R_L$ is the load resistance. Fig. 3 shows the basic equivalent circuit of the SS topology.

For primary current $I_1$, secondary current $I_2$, and secondary voltage $V_2$, the equations are derived as

$$I_1 = \frac{R_2 + R_L + j\left(\omega L_2 - \frac{1}{\omega C_2}\right)}{\left\{R_1 + j\left(\omega L_1 - \frac{1}{\omega C_1}\right)\right\}\left\{R_2 + R_L + j\left(\omega L_2 - \frac{1}{\omega C_2}\right)\right\} + \omega^2 L_m^2} V_1, \quad (1)$$

$$I_2 = \frac{j\omega L_m}{\left\{R_1 + j\left(\omega L_1 - \frac{1}{\omega C_1}\right)\right\}\left\{R_2 + R_L + j\left(\omega L_2 - \frac{1}{\omega C_2}\right)\right\} + \omega^2 L_m^2} V_1, \quad (2)$$

$$V_2 = \frac{j\omega L_m R_L}{\left\{R_1 + j\left(\omega L_1 - \frac{1}{\omega C_1}\right)\right\}\left\{R_2 + R_L + j\left(\omega L_2 - \frac{1}{\omega C_2}\right)\right\} + \omega^2 L_m^2} V_1. \quad (3)$$

Assuming that the resonance frequency is identical on the primary and secondary sides, when the resonance frequency is expressed as eq. (4), the power supplied to the load resistance $P_L$, power efficiency $\eta$, and voltage amplification factor $A_v$, which is the ratio of $V_1$ to $V_2$, are described by the following equations.

$$\omega_0 = \frac{1}{\sqrt{L_1 C_1}} = \frac{1}{\sqrt{L_2 C_2}} \quad (4)$$

$$P_L = \frac{(\omega_0 L_m)^2 R_L}{\{R_1(R_2 + R_L) + (\omega_0 L_m)^2\}^2} V_1^2 \quad (5)$$

$$\eta = \frac{(\omega_0 L_m)^2 R_L}{(R_2 + R_L)\{R_1 R_L + R_1 R_2 + (\omega_0 L_m)^2\}} \quad (6)$$

$$A_v = \frac{\omega_0 L_m R_L}{R_1 R_L + R_1 R_2 + (\omega_0 L_m)^2} \quad (7)$$

Here, by applying partial differentiation of the load resistance on the efficiency, we can determine the value of $R_L$ that maximizes the WPT efficiency $R_{L\eta max}$, which makes the partial derivative zero.

$$\frac{\partial \eta}{\partial R_L} = 0 \Rightarrow R_{L\eta max} = \sqrt{R_2^2 + \frac{R_2(\omega_0 L_m)^2}{R_1}} \quad (8)$$

When the efficiency-maximum load is used, $P_L$, $\eta$, $A_v$ are described by the following equations.

$$P_L = \frac{\sqrt{(R_1 R_2)^2 + R_1 R_2 (\omega_0 L_m)^2}(\omega_0 L_m)^2}{\left((\omega_0 L_m)^2 + R_1 R_2 + \sqrt{(R_1 R_2)^2 + R_1 R_2 (\omega_0 L_m)^2}\right)^2} \frac{V_1^2}{R_1} \quad (9)$$

$$\eta = \frac{(\omega_0 L_m)^2}{\left(\sqrt{R_1 R_2} + \sqrt{R_1 R_2 + (\omega_0 L_m)^2}\right)^2} \quad (10)$$

$$A_v = \sqrt{\frac{R_2}{R_1}} \frac{\omega_0 L_m}{\sqrt{R_1 R_2} + \sqrt{R_1 R_2 + (\omega_0 L_m)^2}} \quad (11)$$

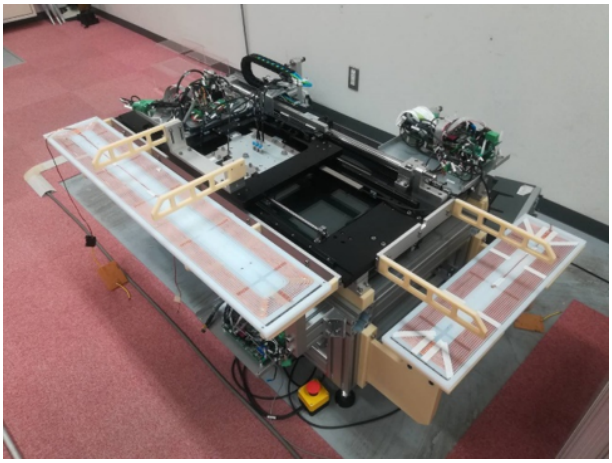

Fig. 4. Overview of WHPS2

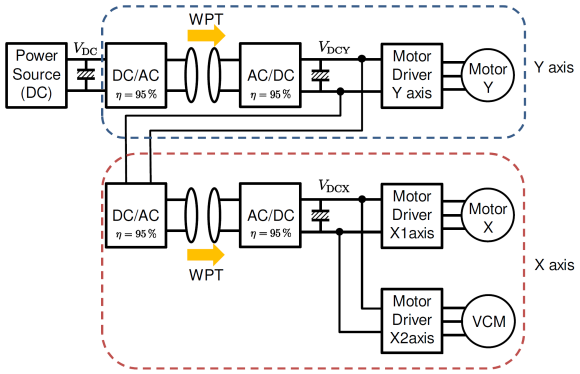


Fig. 5. The structure of WHPS2

### 2.2 Structural description of WHPS

In our group, we constructed a multi-axis wireless high-precision stage (Wireless High Precision Stage 2 : WHPS2). An overview of WHPS2 is shown in Fig. 4. WHPS2 is a two-axis (Y-X) high-precision stage that transfers electric power from power by WPT. Fig. 5 shows the electrical structure of WHPS2. The inverter converts the direc- current voltage source into a rectangular wave oscillating at 85 kHz. The power from the primary side of the Y axis is transferred to the secondary side by WPT. A part of the power transferred to the secondary side drives the linear motor of the Y-axis coarse stage. The rest of the power is transferred to the X-axis of the secondary side, and it drives the linear motor of the X-axis coarse stage and the voice coil motor of the fine stage. Each stage is guided by an air guide, and the position of each stage is measured by linear encoders with a resolution of 4 nm. The voltage of the smoothing capacitor on both the axes should be maintained within a certain range to drive the motor drivers and make the motors move properly. A 2-mode control scheme is adopted to stabilize the voltage. The control method will be described in detail in the next section.

## 3. DC link voltage stabilization control for WPT

**3.1 Instability of CPL on WPT systems** A constant power load (CPL), which includes a linear motor used in WHPS2, is the most difficult load to handle for WPT systems. It has been confirmed experimentally and theoretically

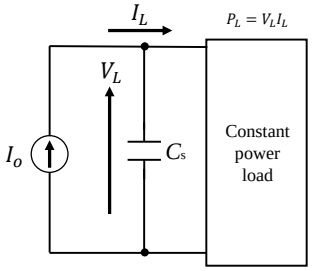


Fig. 6. An equivalent secondary circuit

that the behavior of a WPT system is unstable when a CPL is connected to the secondary side of the WPT system [8] . Fig. 6 shows an equivalent secondary circuit. This circuit diagram regards the primary circuit as an equivalent current source. In this figure, the current from the equivalent current source is $I_o$, the voltage and current of the CPL are $V_L$ and $I_L$, respectively, and the capacitance of the smoothing capacitor is $C_s$. The following circuit equations are derived from the model.

By the kirchhoff's law,

$$I_L = I_o - C_s \frac{dV_L}{dt}. \tag{12}$$

When the power consumed on the load is $P_L$,

$$I_L = \frac{P_L}{V_L}. \tag{13}$$

From eq. (12), eq.(13).

$$\frac{dV_L}{dt} = -\frac{P_L}{C_s V_L} + \frac{I_o}{C_s}. \tag{14}$$

By linearizing eq. (14) around the equilibrium point, eq. (17) is derived.

$$V_L = v_L + \Delta V_L \tag{15}$$

$$I_o = i_o + \Delta i_o \tag{16}$$

$$\frac{d\Delta V_L}{dt} = -\frac{P_L \Delta V_L}{C_s v_L^2} + \frac{\Delta I_o}{C_s} \tag{17}$$

By applying Laplace transform on this equation, the transfer function $P_\Delta(s)$ from $\Delta i_o$ to $\Delta v_2$ eq. (18) is derived as,

$$P_\Delta(s) = \frac{\Delta V_L(s)}{\Delta I_o(s)} = \frac{1}{C_s\left(s - \frac{P_L}{C_s v_L^2}\right)}. \tag{18}$$

The pole of the transfer function $p$ is

$$p = \frac{P_L}{C_s v_L^2}. \tag{19}$$

The system is unstable because the pole is always positive when $P_L > 0$ and $v_L > 0$. The speed of the pole is higher when the following cases:

- Load power $P_L$ is higher.
- The capacitance of the smoothing capacitor $C_s$ is smaller.
- The operating load voltage $v_L$ is greater.

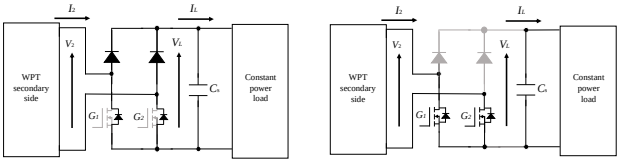


(a)Rectification mode (b)Short mode

Fig. 7. 2 mode control

### 3.2 2 mode control for stability

WPT systems with CPL are unstable, as shown in the previous section. To avoid unstability, a feedback control scheme, called 2-mode control scheme, is often adopted on the secondary converter [9], [10]. This control method has the following two modes:

- Rectification mode: All switching devices are in the OFF state. In this mode, the secondary converter behaves as a full-bridge rectifier, as shown in Fig. 7(a). Hence, power is transferred from the primary side to the load side. In the rectification mode, the load voltage increases if the transferred power is greater than the required power on the load.

- Short mode: Both the lower-arm switching devices are in the ON state. Then, the secondary converter separates the primary side from the load side, as shown in Fig. 7(b). Thus, power is not transferred to the load side. In the short mode, power is provided from the smoothing capacitor, leading to a decrease in the load voltage.

By switching these two modes based on the measured load voltage, the value is maintained within a certain range.

## 4. High efficiency operation of WHPS2

In this paper, the author would like to pursue the high efficiency operation on WHPS2. The power trajectory of the stage is predetermined. Thus, the overall input power should be the lowest when WHPS2 is operating in the most efficient mode in a given situation. The calculation of the overall input power will be described by the following equations.
The input power at an arbitrary moment can be calculated as the product of current and voltage of the power supply. However, the values of current are different for each mode. Thus, the input power in each mode should be calculated separately. The RMS values of the current of the primary side in the short mode $I_{1s}$ and that of the rectification mode $I_{1r}$ are described by the following equations (20),(21).

$$I_{1s} \simeq \frac{R_2 V_{DC}}{R_1 R_2 + (\omega_0 L_m)^2} \tag{20}$$

$$I_{1r} \simeq \frac{R_2 V_{DC} + \frac{2\sqrt{2}}{\pi}\omega_0 L_m V_L}{R_1 R_2 + (\omega_0 L_m)^2} \tag{21}$$

By the equations (20) and (21), the power values supplied by the primary inverter in the short mode $P_{1s}$ and rectification mode $P_{1r}$ are described by the following equations (22), (23) [11]. $P_{1s}$ is consumed in the short mode, and $P_{1r}$ is consumed in the rectification mode. When power is not transferred from the primary side to the load side in the short

mode, all the power supplied by the primary side $P_{1s}$ will be lost. To reduce this loss, the ratio of the rectification mode should be greater during operation.

$$P_{1s} \simeq \frac{R_2 {V_{DC}}^2}{R_1 R_2 + (\omega_0 L_m)^2} \tag{22}$$

$$P_{1r} \simeq \frac{R_2 V_{DC} + \frac{2\sqrt{2}}{\pi}\omega_0 L_m V_L}{R_1 R_2 + (\omega_0 L_m)^2} V_{DC} \tag{23}$$

The RMS value of the input voltage $V_1$ is calculated by the fourier series of the input DC voltage $V_{DC}$.

$$V_{DC} = \frac{2\sqrt{2}}{\pi} V_1 \tag{24}$$

Here, to calculate the overall input power, the ratio of the short mode and the rectification mode should be considered. The ratio of the short mode $m_p$ is given by the following equationsy(26), (25).

$$m_p = \frac{t_s}{t_s + t_r} \tag{25}$$

$$m_p = \frac{\ln(\frac{V_{low}}{V_{up}})}{\ln(\frac{V_{low}}{V_{up}}) + \ln(\frac{V_{up}+R_L I_a}{V_{low}-R_L I_a})} \tag{26}$$

$V_{up}$ is the upper limit of the 2-mode control scheme, and $V_{low}$ is the lower limit. $I_a$ here means the output current of the secondary converter, and the value is described by the following equation (27).

$$I_a = \frac{2\sqrt{2}}{\pi} \frac{\omega_0 L_m V_{DC} - \frac{2\sqrt{2}}{\pi} R_1 V_L}{R_1 R_2 + (\omega_0 L_m)^2} \tag{27}$$

$t_s$ and $t_r$ are the durations of the short mode and the rectification mode in a resonance cycle, respectively. By using these equations of power and time in each mode, the input power is derived by eq. (28).

$$P_1 = m_p P_{1s} + (1 - m_p) P_{1r} \tag{28}$$

The overall input power is the integral value of $P_1$. Thus, the integral value is low when high-efficiency control is in operation because the required power is the same for both experimental conditions.

## 5. Input voltage control based on power trajectory

The proposed method increases, the rectification ratio by power transfer capability adjustment based on the input voltage $V_1$ is proposed.The power transfer capability is derived from the input voltage $V_1$. The relationship between them is expressed by the following equation (29) [12].

$$V_1 = \frac{R_1}{\omega_0 L_m} \left\{ V_2 + \frac{(1 + \frac{L_m^2 \omega_0^2}{R_1 R_2}) R_2 P_L}{V_2} \right\} \tag{29}$$

The conventional and proposed method are shown in Fig. 8. The required power trajectory of the high-precision stage is predetermined. For the predetermined trajectory, the input voltage values $V_1$ are determined for the proposed method.

Table 1. Comparison of the two methods

| Subject | $V_1$ | $V_L$ | Short mode loss | WPT efficiency |
|---|---|---|---|---|
| Conventional | Constant | 2 mode | High | Low |
| Proposed | Time-variant | 2 mode | Low | High |

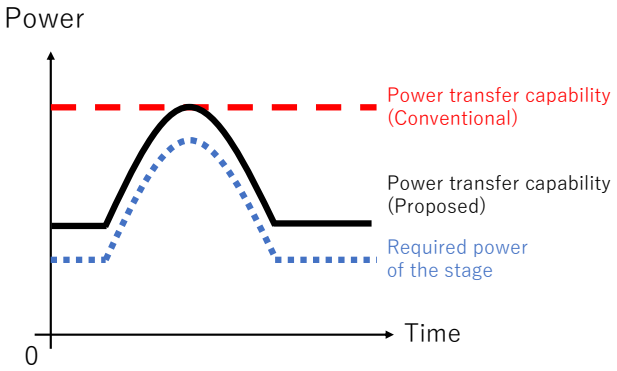


Fig. 8. Conventional and proposed method

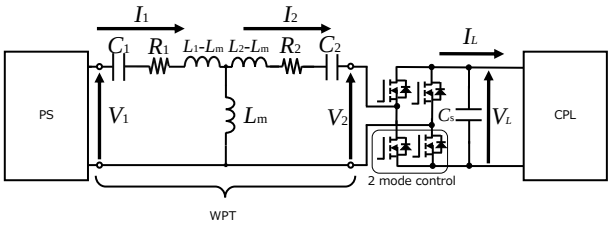


Fig. 9. Simulation model

Conventional Method : A constant input voltage is applied. The voltage is predetermined to match the power transfer capability with the 200% of the peak value of the required power. The value of $V_2$ is chosen to match the relationship which can achieve the theoretical maximum WPT transfer efficiency. However, the ratio between the short mode time and rectification mode time is not so desirable since the short mode is long, therefore the energy loss caused by being in short mode would be high.

Proposed Method : Time-variant $V_1$ is used in this method. As shown in Fig. 8, the power transfer capability is slightly larger than the required power at all times. By using this control scheme, the short mode time would be shorter, but the WPT efficiency will be lower than that of the conventional method.

The advantages and disadvantages of both the methods are summarized in Table 1.

## 6. Simulation

**6.1 Simulation conditions** The simulations were implemented in MATLAB Simulink Power Systems. The model for the simulations is shown in Fig.9. The trajectory used is shown in Fig.10. In the power trajectory, the black line denotes the actual power trajectory and the red line denotes the target trajectory of the power transfer capability. To avoid unstability, 200% of the actual power trajectory is used for the power transfer capability because of the shortage of transferred power. The constants for the simulations are listed in Table.2.

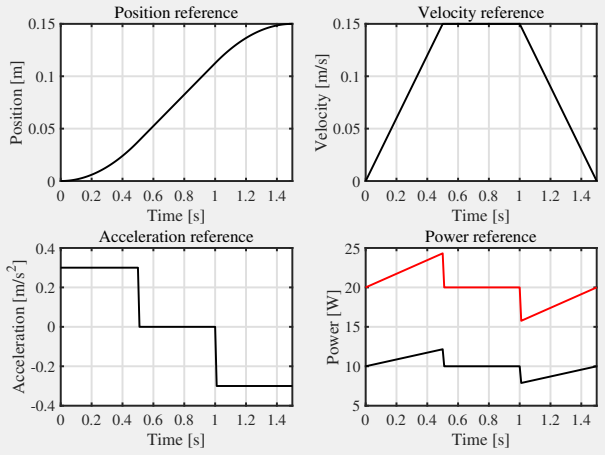


Fig. 10. Trajectory

Table 2. Constants in the simulation

| Constant | Value |
|---|---|
| Primary resistance $R_1$ | 0.596 Ω |
| Secondary resistance $R_2$ | 0.367 Ω |
| Primary inductance $L_1$ | 85.0 $\mu$H |
| Secondary inductance $L_2$ | 50.0 $\mu$H |
| Primary capacitor $C_1$ | 41.2 nF |
| Secondary capacitor $C_2$ | 70.1 nF |
| Mutual inductance $L_m$ | 25.0 $\mu$H |
| Frequency $f$ | 85.0 kHz |
| Smoothing capacitor $C_s$ | 1.00 mF |
| Upper limit of 2 mode $V_{up}$ | 24.9 V |
| Lower limit of 2 mode $V_{low}$ | 23.9 V |

- Conventional Method :
  Constant $V_1$ (The $V_1$ to match the peak of the power trajectory with the transfer ability with a certain margin)

- Proposed Method :
  Time-variant $V_1$ to increase the rectification mode ratio. By doing so, the loss caused by the short mode will decrease. However, the WPT efficiency is slightly lower than that of the conventional method.

### 6.2 Simulation results

The simulation results are shown in Fig. 11. In (a), the power trajectory of the load and the power transfer capability values are shown. In (b), the WPT efficiency of each method only in rectification mode is shown. The conventional method maintains the maximum WPT efficiency in all range of operation. Therefore, the loss caused by the WPT efficiency in the proposed method is greater than that in the conventional method. In (c) and (d), the supplied power trajectories of the primary inverter are shown for each method. In (e), the ratio of the rectification mode 1-$m_p$ is shown. For the proposed method, the ratio is much higher than that for the conventional method when the required power of the stage is not much. This means that the energy consumed by its short mode is lower. Taking these results into consideration, the input power of each method and the required power can be compared as shown in (f). In (f), the conventional method requires more power for the same power trajectories, which means that the proposed method surpasses the conventional method.

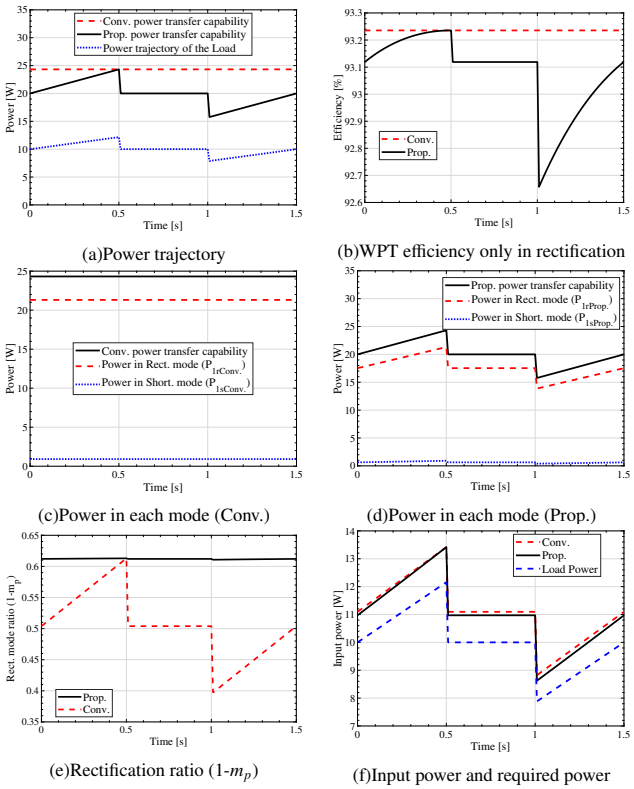


Fig. 11. Simulation results

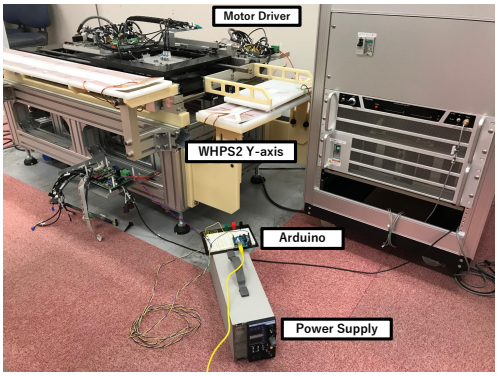


Fig. 12. Experimental setup

In this simulation, only steady-states of two-mode operations are considered; therefore, the exact values of the required power cannot be determined easily.

## 7. Experiments

### 7.1 Setup

The experiments are performed by WHPS2 of The University of Tokyo. The setup of the experiment is shown in Fig. 12. The time-variant input voltage is applied to the primary side of the Y-axis of WHPS2 from the power supply and only the Y-axis is used in the experiment. The signal for controlling the input voltage of the power supply is sent from an Arduino. The time-variant input power is transferred to the motor driver for actuation. Each value of the input voltage and the input current is measured to calculate the input power.

### 7.2 Experimental results

The experimental results are shown in Fig. 13. In (a), the

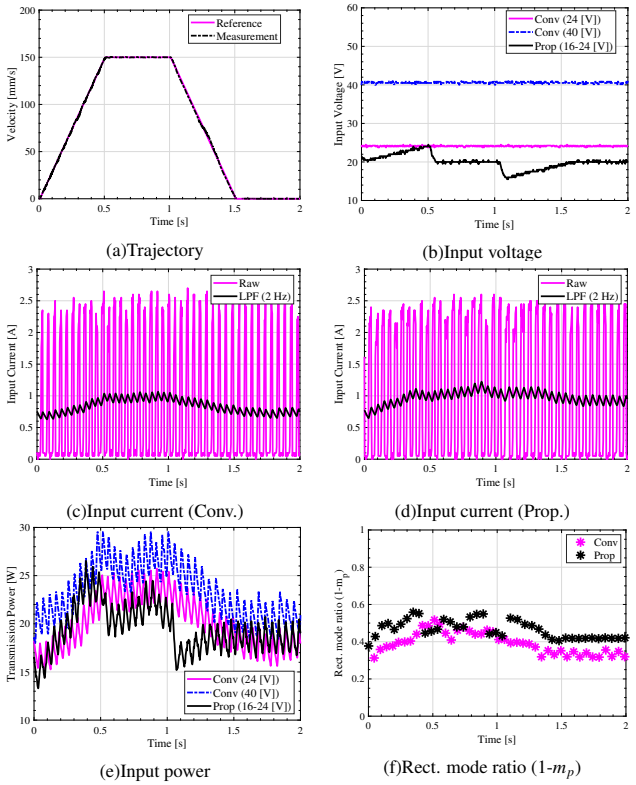


Fig. 13. Experimental results

target trajectory and the actual one are shown. The actual trajectory is nearly the same as the target trajectory. The trajectory consists of a 0.5-s acceleration range, a 0.5-s fixed-speed range, and a 0.5-s deceleration. The maximum speed is 150 mm/s. In (b), the input voltage profiles are shown. In (c) and (d), the input current of each method is shown. In (e), the input power trajectories are shown. By using these results, the overall input power of the trajectory is calculated and integrated for 2 s, as listed in Table. 3. By this comparison, the proposed method can reduce 3.5 % of the overall input power compared with the conventional (24 V). The average consumed power on the stage is predetermined and the experimental condition is the same for the three methods, excluding the input voltage, and the proposed method surpasses these two conventional methods. The results suggest that the input power of the proposed method goes greatly under the conventional one when the stage is about to decelerate. However, in some range, the conventional method surpasses the proposed method; therefore, further method to determine the input voltage trajectory should be investigated for higher efficiency. For example, the modeling of the required power should be discussed in more detail like the effects of the viscous resistance or the inertial resistance and so on. In(f), the rectification ratios are shown. It can be seen that the rectification ratio of the proposed method is higher than the conventional one for almost entire range.

Table 3. Input power comparison

| Subject | Input power [J] |
|---|---|
| Conventional (40V) | 23.4 |
| Conventional (24V) | 20.2 |
| Proposed (16V-24V) | 19.5 |

## 8. Conclusion

To enhance the efficiency of a high-precision stage without cable disturbance, we proposed a new control scheme on input voltage, considering the power trajectory of the stage. The proposed method employed time-variant input voltage to manipulate the transmission power capability of WHPS2. Through experiments, the effectiveness of the proposed method was validated and the effectiveness of the proposed method was calculated such that it could reduce 3.5 % of the overall input power compared with the conventional method. However, for further efficiency, more detailed modeling of the required power of the stage should be discussed. In conclusion, the decision of the input power trajectory is important for wireless powered high-precision stages for high efficiency operation.

## Acknowledgement

This work was partly supported by JSPS KAKENHI Grant Number 18H03768.

## References

( 1 ) W. Ohnishi and H. Fujimoto, “Decoupling Control for High-Precision Stages by the Center of Rotation and Gravity Hybrid-Driven Method using Multiple Actuators,” pp. 2–5.

( 2 ) K. Sakata, H. Fujimoto, A. Hara, and K. Saiki, “Design fabrication of high-precision stage and ultrahigh-speed nanoscale positioning,” *Proceedings of the American Control Conference*, pp. 2254–2259, 2009.

( 3 ) W.-j. Kim, T. Hu, and N. D. Bhat, “Design and Control of a 6-DOF High-Precision Integrated Positioner,” *Proceedings of the 2004 American Control Conference*, pp. 2493–2498, 2004.

( 4 ) T. Oomen, R. Van Herpen, S. Quist, M. Van De Wal, O. Bosgra, and M. Steinbuch, “Connecting system identification and robust control for next-generation motion control of a wafer stage,” *IEEE Transactions on Control Systems Technology*, vol. 22, no. 1, pp. 102–118, 2014.

( 5 ) M. Sato, G. Yamamoto, D. Gunji, T. Imura, and H. Fujimoto, “Development of Wireless In-Wheel Motor Using Magnetic Resonance Coupling,” *IEEE Transactions on Power Electronics*, vol. 31, no. 7, pp. 5270–5278, 2016.

( 6 ) D. Patil, M. K. McDonough, J. M. Miller, B. Fahimi, and P. T. Balsara, “Wireless Power Transfer for Vehicular Applications: Overview and Challenges,” *IEEE Transactions on Transportation Electrification*, vol. 4, no. 1, pp. 3–37, 2017.

( 7 ) A. Kurs, A. Karalis, R. Moffatt, J. D. Joannopoulos, P. Fisher, and M. Soljačić, “Wireless power transfer via strongly coupled magnetic resonances,” *Science*, vol. 317, no. 5834, pp. 83–86, 2007.

( 8 ) D. Gunji and T. Imura, “Stability Analysis of Secondary Load Voltage on Wireless Power Transfer using Magnetic Resonance Coupling for Constant Power Load,” no. 5.

( 9 ) D. Gunji, T. Imura, and H. Fujimoto, “Stability analysis of constant power load and load voltage control method for Wireless In-Wheel Motor,” *9th International Conference on Power Electronics - ECCE Asia: "Green World with Power Electronics", ICPE 2015-ECCE Asia*, pp. 1944–1949, 2015.

(10) G. Lovison, D. Kobayashi, M. Sato, T. Imura, and Y. Hori, “Secondary-side-only Control for High Efficiency and Desired Power with Two Converters in Wireless Power Transfer Systems,” *IEEJ Journal of Industry Applications*, vol. 6, no. 6, pp. 473–481, 2017. [Online]. Available: https://www.jstage.jst.go.jp/article/ieejjia/6/6/6{_}473/{_}article

(11) Y. Gaku, I. Takehiro, and F. Hiroshi, “Basic Study on Maximizing Power Transfer Efficiency of Wireless In-wheel Motor by Primary and Load-Side Voltage Control,” *Technical Committee on Semiconductor Power Converter IEEJ Industry Applications Society*, no. 9, pp. 83–88, 2015.

(12) Y. H. Katsuhiro Hata, Takehiro Imura, “Proposal of Classification and Design Strategies for Wireless Power Transfer Based on Specification on Transmitter-Side and Receiver-Side Voltages and Power Requirements,” *IEEJ Transactions on Industry Applications*, pp. 1–10, 2018.